ISSN 2176-5480

22nd International Congress of Mechanical Engineering (COBEM 2013)
November 3-7, 2013, Ribeirão Preto, SP, Brazil

VERIFICATION AND VALIDATION OF A DIRECT NUMERICAL SIMULATION CODE FOR TRANSITIONAL BOUNDARY LAYER

Larissa Alves Petri
Leandro Franco de Souza
Institute of Mathematical and Computer Sciences, University of São Paulo. São Carlos-SP, Brazil.
lariss@gmail.com, lefraso@gmail.com

Abstract. *Numerical results from the Direct Numerical Simulation (DNS) code are compared in a boundary layer over an airfoil with experimental and Linear Stability Theory (LST) results. Characteristics from the boundary layer, as displacement thickness, momentum thickness and shape factor, are taken into consideration. Comparisons considering the amplitude of the velocity disturbance caused by two-dimensional Tollmien-Schlichting waves are also made. The results shows that the DNS code is verified and validated.*

Keywords: *boundary layer, incompressible flow, high-order compact finite differences, direct numerical simulation, verification and validation*

1. INTRODUCTION

The no-slip condition on a solid body reduces the velocities in the outer flow to zero on the surface. This reduction generates large velocity gradients in a thin layer adjacent to the surface of the body. This layer is the boundary layer, in which strong viscous effects exist (Currie, 2003).

The boundary layer is directly affected by the outer flow (Reed *et al.*, 1996; White, 2006). The presence of a favorable pressure gradient causes the outer flow to accelerate and stabilizes the boundary layer flow. On the other hand, the presence of an adverse pressure gradient decelerates the outer flow and increases the instability of the boundary layer.

An increasing instability leads to transition to turbulence and predicting the location of the transition point is still a challenge. Experimental and numerical studies are being used to explain and predict this phenomenon.

In this paper, the results carried out by a Direct Numerical Simulation (DNS) code are compared to experimental and Linear Stability Theory (LST) ones in order to verify and validate the code. The experimental results were obtained at the wind tunnel of the Institute of Aerodynamics and Gas Dynamics of the University of Stuttgart. The formation of the boundary layer is validated by means of comparisons involving the following parameters: streamwise velocity at the boundary layer edge, displacement thickness, momentum thickness and shape factor are presented.

Small disturbances produces Tollmien-Schlichting (TS) waves in the flow. The growth or decay of this waves indicates if the flow is stable or unstable. According to linear stability theory, when the amplitudes of this waves are small, they can grow until certain point (neutral curve) and starts to decay. Based on this, TS waves were introduced on the flow, in order to study the disturbance caused by them in the velocity profile. The amplitude of the disturbance in the streamwise direction was also compared between experimental, LST and numerical results with the aim of verifying and validating the DNS code.

2. FORMULATION

In this section the governing equations and the numerical methodology implemented are presented. The governing equations are based on Navier-Stokes equations, written in the vorticity-velocity formulation. The discretization is carried out by means of high-order finite-differences schemes and spectral approximations for the spatial derivatives and a fourth order Runge-Kutta scheme for the temporal discretization.

2.1 Governing equations

The governing equations are the incompressible equations with constant viscosity, based on Navier-Stokes equations written in orthogonal coordinates. Defining the vorticity as the negative curl of the velocity vector, and using the fact that both the velocity and the vorticity fields are solenoidal, one can obtain the following vorticity transport equation in each direction:

$$\frac{\partial \omega_x}{\partial t} + \frac{\partial a}{\partial y} - \frac{\partial b}{\partial z} = \nabla^2 \omega_x, \tag{1}$$

$$\frac{\partial \omega_y}{\partial t} + \frac{\partial c}{\partial z} - \frac{\partial a}{\partial x} = \nabla^2 \omega_y, \tag{2}$$

ISSN 2176-5480

$$\frac{\partial \omega_z}{\partial t} + \frac{\partial b}{\partial x} - \frac{\partial c}{\partial y} = \nabla^2 \omega_z, \tag{3}$$

where

$$a = \omega_x v - \omega_y u, \tag{4}$$

$$b = \omega_z u - \omega_x w, \tag{5}$$

$$c = \omega_y w - \omega_z v, \tag{6}$$

are the nonlinear terms resulting from convection, vortex stretching and vortex bending. The variables u, v, w, ω_x, ω_y, ω_z are the velocity and vorticity components in the streamwise (x), wall-normal (y) and spanwise (z) directions respectively; t is the time. The Laplace operator is:

$$\nabla^2 = \frac{1}{Re}\left(\frac{\partial^2}{\partial x^2} + \frac{\partial^2}{\partial z^2}\right) + \frac{\partial^2}{\partial y^2}. \tag{7}$$

The continuity equation is given by:

$$\frac{\partial u}{\partial x} + \frac{\partial v}{\partial y} + \frac{\partial w}{\partial z} = 0. \tag{8}$$

The above equations are presented in a non-dimensional form. The reference length is a plate-characteristic length $\tilde{L}$ and the reference velocity is the free stream velocity $\tilde{U}_\infty$. The Reynolds number is given by

$$Re = \frac{\tilde{U}_\infty \tilde{L}}{\tilde{\nu}}, \tag{9}$$

where $\tilde{\nu}$ is the kinematic viscosity.

The variables are non-dimensionalized according to:

$$x = \frac{x^*}{L}; \quad y = \frac{y^*\sqrt{Re}}{L}; \quad z = \frac{z^*}{L}; \quad u = \frac{u^*}{U_\infty}; \quad v = \frac{v^*\sqrt{Re}}{U_\infty}; \quad w = \frac{w^*}{U_\infty}; \tag{10}$$

$$\omega_x = \frac{\omega_x^* L}{U_\infty \sqrt{Re}}; \quad \omega_y = \frac{\omega_y^* L}{U_\infty}; \quad \omega_z = \frac{\omega_z^* L}{U_\infty \sqrt{Re}}; \quad t = \frac{t^* U_\infty}{L}. \tag{11}$$

Taking the definition of the vorticity and the mass conservation equation, one can obtain Poisson-type equations for each velocity component:

$$\frac{\partial^2 u}{\partial x^2} + \frac{\partial^2 u}{\partial z^2} = -\frac{\partial \omega_y}{\partial z} - \frac{\partial^2 v}{\partial x \partial y}, \tag{12}$$

$$\frac{1}{Re}\left(\frac{\partial^2 v}{\partial x^2} + \frac{\partial^2 v}{\partial z^2}\right) + \frac{\partial^2 v}{\partial y^2} = -\frac{\partial \omega_z}{\partial x} + \frac{\partial \omega_x}{\partial z}, \tag{13}$$

$$\frac{\partial^2 w}{\partial x^2} + \frac{\partial^2 w}{\partial z^2} = \frac{\partial \omega_y}{\partial x} - \frac{\partial^2 v}{\partial y \partial z}. \tag{14}$$

3. NUMERICAL METHOD

The equations presented above are discretized by high-order finite differences schemes and spectral approximations for the spatial derivatives. A fourth-order four-step Runge-Kutta method is used for the temporal discretization.

3.1 Discretization of field equations

The flow is assumed to be periodic in the spanwise direction. Therefore, the flow field can be expanded in Fourier series with K spanwise Fourier modes:

$$f(x, y, z, t) = \sum_{k=0}^{K} F_k(x, y, t) e^{(i\beta_k z)} \tag{15}$$

ISSN 2176-5480

where

$$f = u, v, w, \omega_x, \omega_y, \omega_z, a, b, c, \tag{16}$$

$$F_k = U_k, V_k, W_k, \Omega_{x_k}, \Omega_{y_k}, \Omega_{z_k}, A_k, B_k, C_k, \tag{17}$$

and β_k is the spanwise wavenumber given by

$$\beta_k = \frac{2\pi k}{\lambda_z}, \tag{18}$$

and λ_z is the spanwise wavelength of the fundamental spanwise Fourier mode, and $i = \sqrt{-1}$. Note that F_k may be fully complex, i.e., non-symmetric three-dimensional disturbance fields can be computed. The nonlinear terms are computed pseudospectrally, i.e. by transformation of all flow variables to physical space, computing the nonlinear terms at consecutive spanwise stations, and transforming the products back to Fourier space.

Substituting the Fourier transforms (Eq. (15)) in the vorticity transport equations (Eq. (1) – Eq. (3)) and in the velocity Poisson equations (Eq. (12) – Eq. (14)) yield the governing equations in the Fourier space, for each Fourier mode:

$$\frac{\partial \Omega_{x_k}}{\partial t} + \frac{\partial A_k}{\partial y} - \beta_k B_k = \nabla_k^2 \Omega_{x_k}, \tag{19}$$

$$\frac{\partial \Omega_{y_k}}{\partial t} + \beta_k C_k - \frac{\partial A_k}{\partial x} = \nabla_k^2 \Omega_{y_k}, \tag{20}$$

$$\frac{\partial \Omega_{z_k}}{\partial t} + \frac{\partial B_k}{\partial x} + \frac{\partial C_k}{\partial y} = \nabla_k^2 \Omega_{z_k}, \tag{21}$$

$$\frac{\partial^2 U_k}{\partial x^2} - \beta_k^2 U_k = -\beta_k \Omega_{y_k} - \frac{\partial^2 V_k}{\partial x \partial y}, \tag{22}$$

$$\frac{1}{Re}\left(\frac{\partial^2 V_k}{\partial x^2} - \beta_k^2 V_k\right) + \frac{\partial^2 V_k}{\partial y^2} = -\frac{\partial \Omega_{z_k}}{\partial x} + \beta_k \Omega_{x_k}, \tag{23}$$

$$\frac{\partial^2 W_k}{\partial x^2} - \beta_k^2 W_k = \frac{\partial \Omega_{y_k}}{\partial x} + \beta_k \frac{\partial V_k}{\partial y}, \tag{24}$$

where

$$\nabla_k^2 = \frac{1}{Re}\left(\frac{\partial^2}{\partial x^2} - \beta_k^2\right) + \frac{\partial^2}{\partial y^2}. \tag{25}$$

The equations (Eq. (19) – Eq. (24)) are solved numerically in the domain shown schematically in Fig. 1. The calculations are done on an orthogonal uniform grid, parallel to the wall. The fluid enters the computational domain at $x = x_0$ and exits at the outflow boundary $x = x_{max}$. Disturbances are introduced into the flow field using spanwise suction and blowing in a disturbance strip at the wall. This strip is located between x_1 and x_2. In the region located between x_3 and x_4 a buffer domain technique, from Kloker and Konzelmann (1993), is implemented in order to avoid wave reflections at the outflow boundary. In these simulations a Falkner-Skan boundary layer is used as the base flow.

The time derivatives in the vorticity transport equations are discretized with a classical fourth-order Runge-Kutta integration scheme (Ferziger and Peric, 1997). The spatial derivatives are calculated using a high-order compact finite difference schemes (Souza *et al.*, 2005; Souza, 2003; Kloker, 1998; Lele, 1992). The V-Poisson equation (Eq. (23)) is solved using a multigrid Full Approximation Scheme (FAS) (Stüben and Trottenberg, 1981). A V-cycle with 4 grids is implemented. The code is parallelized, using domain decomposition in the streamwise direction.

3.2 Boundary conditions

At the wall ($y = 0$), a no-slip condition is imposed for the streamwise (U_k) and the spanwise (W_k) velocity components. The wall-normal velocity component at the wall (V_k) is specified at the suction and blowing strip regions, where the disturbances are introduced. Away from the disturbance generator this velocity component is set to zero. The function used for the wall-normal velocity at the disturbance generator strip is:

$$V_k(x, 0, t) = A_k f_p(x) \sin(\omega_{t_k} t + \theta_k) \qquad \text{for} \qquad x_1 \leq x \leq x_2, \tag{26}$$

where A_k and θ_k are real constants chosen to adjust the amplitude and phase of the disturbance and ω_{t_k} is the dimensionless frequency. The function $f_p(x)$ adopted is a ninth-order function. This function is used in order to make sure that, at

ISSN 2176-5480

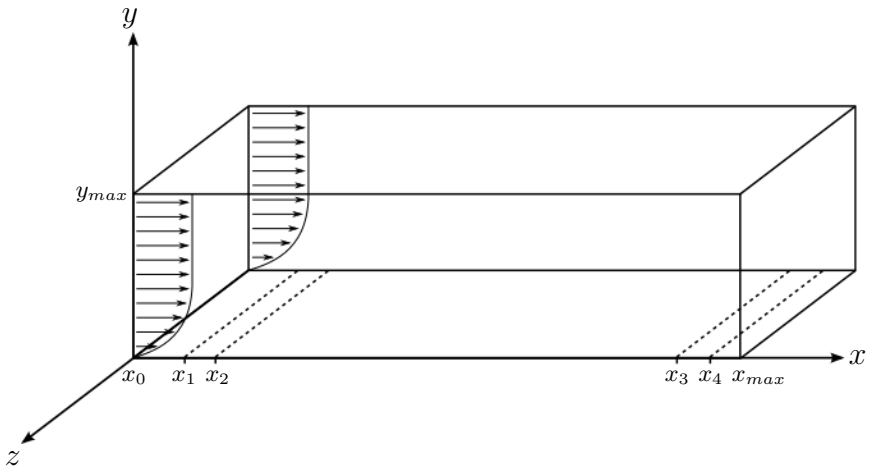

Figure 1. Computational domain.

$y = 0$, the vertical velocity component, its first and second derivatives do not have a discontinuity going in and out of the suction and blowing region.

At the inflow boundary ($x = x_0$), the velocity and vorticity components are specified based on the Falkner-Skan boundary layer solution. At the outflow boundary ($x = x_{max}$), the second derivatives with respect to the streamwise direction of the velocity and vorticity components are set to zero. At the upper boundary ($y = y_{max}$) the flow is considered non rotational. This is satisfied by setting all vorticity components and their derivatives to zero. The wall-normal velocity component at the upper boundary is settled according to the condition:

$$\frac{\partial V_k}{\partial y}|_{x,y_{max},t} = -\frac{\alpha^*}{\sqrt{Re}} V_k(x, y_{max}, t), \tag{27}$$

where $\alpha^* = \sqrt{\alpha^2 + k^2\beta^2}$.

In addition, at the wall ($y = 0$), the condition

$$\frac{\partial V_k}{\partial y} = 0 \tag{28}$$

is imposed in the solution of the Poisson equation (Eq. (22)), to ensure mass conservation. The equations used for evaluating the vorticity components at the wall are:

$$\frac{\partial^2 \Omega_{x_k}}{\partial x^2} - \beta_k^2 \Omega_{x_k} = -\frac{\partial^2 \Omega_{y_k}}{\partial x \partial y} - \beta_k \nabla_k^2 V_k, \tag{29}$$

$$\frac{\partial \Omega_{z_k}}{\partial x} = \beta_k \Omega_{x_k} - \nabla_k^2 V_k. \tag{30}$$

A damping zone near the outflow boundary is defined in which all the disturbances are gradually damped down to zero (Kloker and Konzelmann, 1993). This technique is used to avoid reflections in the outflow boundary. The basic idea is to multiply the vorticity components by a ramp function $f_1(x)$ after each sub-step of the integration method. Using this technique, the vorticity components are taken as:

$$\Omega_k(x, y, t) = f_1(x)\Omega_k^*(x, y, t), \tag{31}$$

where $\Omega_k^*(x, y, t)$ is the disturbance vorticity component that results from the Runge-Kutta integration and $f_1(x)$ is a ramp function that goes from 1 to 0. The implemented function is:

$$f_1(x) = f_1(\epsilon) = (1 - \epsilon^{50})^4 e^{-\frac{\epsilon^3}{10}}, \tag{32}$$

where

$$\epsilon = \frac{x - x_3}{x_4 - x_3} \tag{33}$$

for $x_3 \leq x \leq x_4$. To ensure good numerical results and efficiency a minimum distance between x_3 and x_4 and between x_4 and the end of the domain x_{max} had to be studied. In the present study, 100 points between x_3 and x_4 and 40 points between x_4 and x_{max} were considered.

ISSN 2176-5480

Another buffer domain, located near the inflow boundary is also implemented in the code. As pointed out by Meitz (1996), in simulations involving streamwise vortices, reflections due to the vortices at the inflow can contaminate the numerical solution. The damping function is similar to the one used for the outflow boundary:

$$f_2(x) = f_2(\epsilon) = 6\epsilon^5 - 15\epsilon^4 + 10\epsilon^3 \tag{34}$$

where

$$\epsilon = \frac{x - x_0}{x_1 - x_0} \tag{35}$$

for the range $x_0 \leq x \leq x_1$. All vorticity components are multiplied by this function in this region.

4. RESULTS

In this section, the validation of the DNS code is shown, by means of comparisons between experimental and numerical results. In Sec. 4.1 boundary layer characteristics are compared and in Sec. 4.2 the variation of the amplitude of the streamwise velocity disturbance, caused by Tollmien-Schlichting (TS) waves in the boundary layer, are presented.

The experimental results were performed in the laminar wind tunnel of the Institute of Aerodynamics and Gas Dynamics (IAG) of the University of Stuttgart (Plogmann *et al.*, 2012). The numerical results were obtained during an exchange period at the University of Stuttgart.

4.1 Boundary layer parameters

The formation of the boundary layer is analyzed in this section comparing some boundary layer characteristics. The characteristics considered here are the following: streamwise component of velocity at the boundary layer edge, displacement thickness, momentum thickness and shape factor.

The numerical results consists of two items. The first one is a similarity solution of the Falkner-Skan equation. For this solution, the streamwise velocity component at the boundary layer edge given by the experiments was taken as boundary condition at the upper boundary. This Falkner-Skan solution was considered as initial condition for the second numerical result: a two-dimensional DNS simulation.

In the 2D-DNS code the following parameters were considered: length scale $\tilde{L} = 0.18$m, kinematic viscosity $\tilde{\nu} = 1.56 \times 10^{-5}$m^2/s, domain size 1177×177 points in streamwise and wall-normal directions, respectively, grid space $dx = 3.125 \times 10^{-3}$ and $dy_0 = 1.8 \times 10^{-4}$ in streamwise and wall-normal directions, respectively, with stretching of mesh in wall-normal direction of 1%.

For these comparisons three cases were considered: a flow with pressure gradient close to zero, a decelerated flow and an accelerated flow. This cases were obtained varying the airfoil angle of attack in the experiments.

The velocity scale for non-dimensionalization at each case was: $\tilde{U}_{\infty,x_0} = 29.4985$m/s for the flow with pressure gradient close to zero, $\tilde{U}_{\infty,x_0} = 31.1288$m/s for the decelerated flow and $\tilde{U}_{\infty,x_0} = 27.935$m/s for the accelerated flow, where $\tilde{U}_{\infty,x_0} = \tilde{U}_\infty|_{x_0}$, i. e., $\tilde{U}_\infty$ at the initial point of the domain.

First of all, the streamwise velocity component u in streamwise direction x at the edge of the boundary layer was compared. This result is shown in Fig. 2, for the three pressure distributions considered. u values are non-dimensionalized by $\tilde{U}_{\infty,x_0}$, for each flow type, and x values are non-dimensionalized by $\tilde{L}$.

It is possible to see that all numerical results are close to the experimental ones. Moreover, the velocity behavior shows the variation in the velocity due to the pressure distribution for each case.

For the other characteristics, four results are presented: experimental, theoretical boundary layer profile, Falkner-Skan similarity solution and 2D-DNS. The theoretical boundary layer profile uses the finite difference scheme given by Cebeci and Smith (1974). For the flow with pressure gradient close to zero there are two experimental results.

The second boundary layer characteristic compared is the displacement thickness, given by:

$$\delta_1 = \int_{y=0}^{\infty} \left(1 - \frac{u}{\tilde{U}_\infty}\right) dy. \tag{36}$$

The displacement thickness δ_1 by the streamwise direction x is shown in Fig. 3. δ_1 and x values are non-dimensionalized by $\tilde{L}$.

The four results present a similar behavior for all cases. One can notice that the experimental value tend to be smaller than the numerical ones, when moving away from the leading edge. This phenomenon was observed in other works, however, its causes are still not known.

The next characteristic taken into account is the momentum thickness, obtained by:

$$\delta_2 = \frac{u}{\tilde{U}_\infty} \int_{y=0}^{\infty} \left(1 - \frac{u}{\tilde{U}_\infty}\right) dy. \tag{37}$$

ISSN 2176-5480

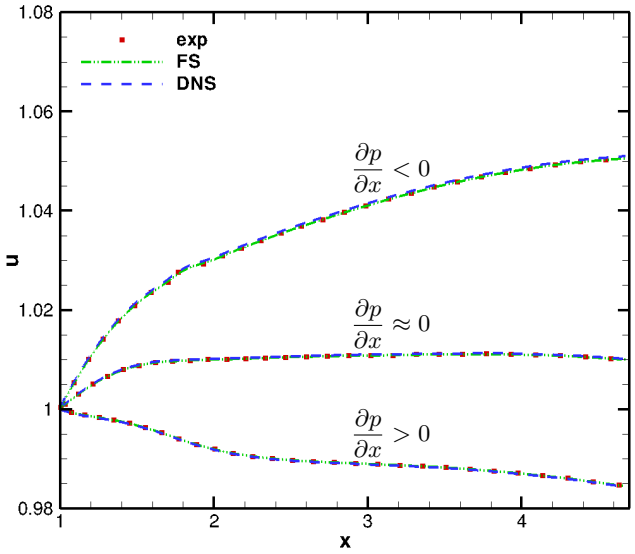

Figure 2. Streamwise velocity u in streamwise direction x at the boundary layer edge for all cases. Exp: experimental, FS: Falkner-Skan solution, DNS: 2D-DNS result.

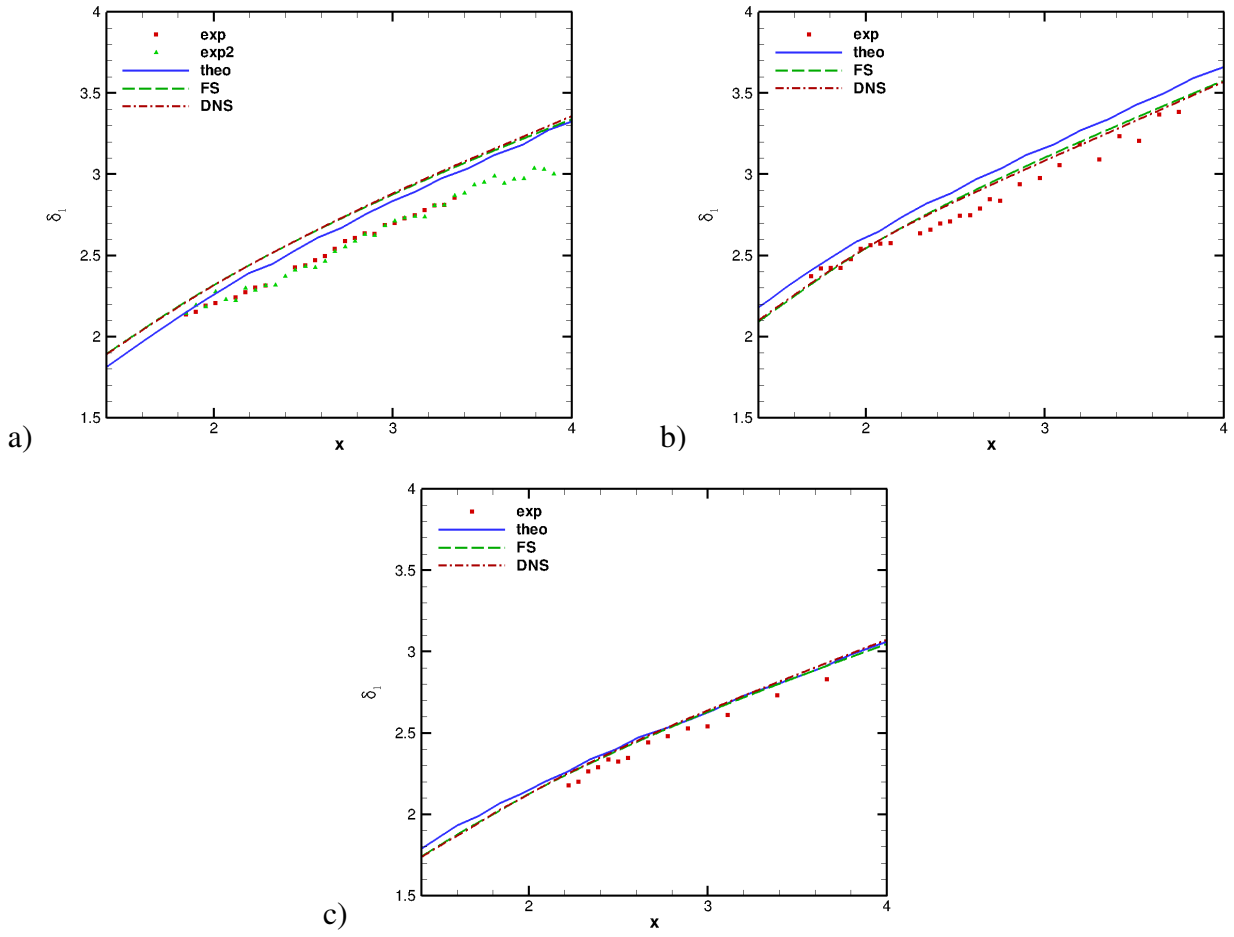

Figure 3. Displacement thickness δ_1 in streamwise direction x, a) flow with pressure gradient close to zero, b) decelerated flow, c) accelerated flow. Exp: experimental, theo: theoretical boundary layer profile, FS: Falkner-Skan solution, DNS: 2D-DNS result.

The comparisons between the momentum thickness in streamwise direction for all cases are presented in Fig. 4. The length scale $\tilde{L}$ is used to non-dimensionalize δ_2 and x values.

ISSN 2176-5480

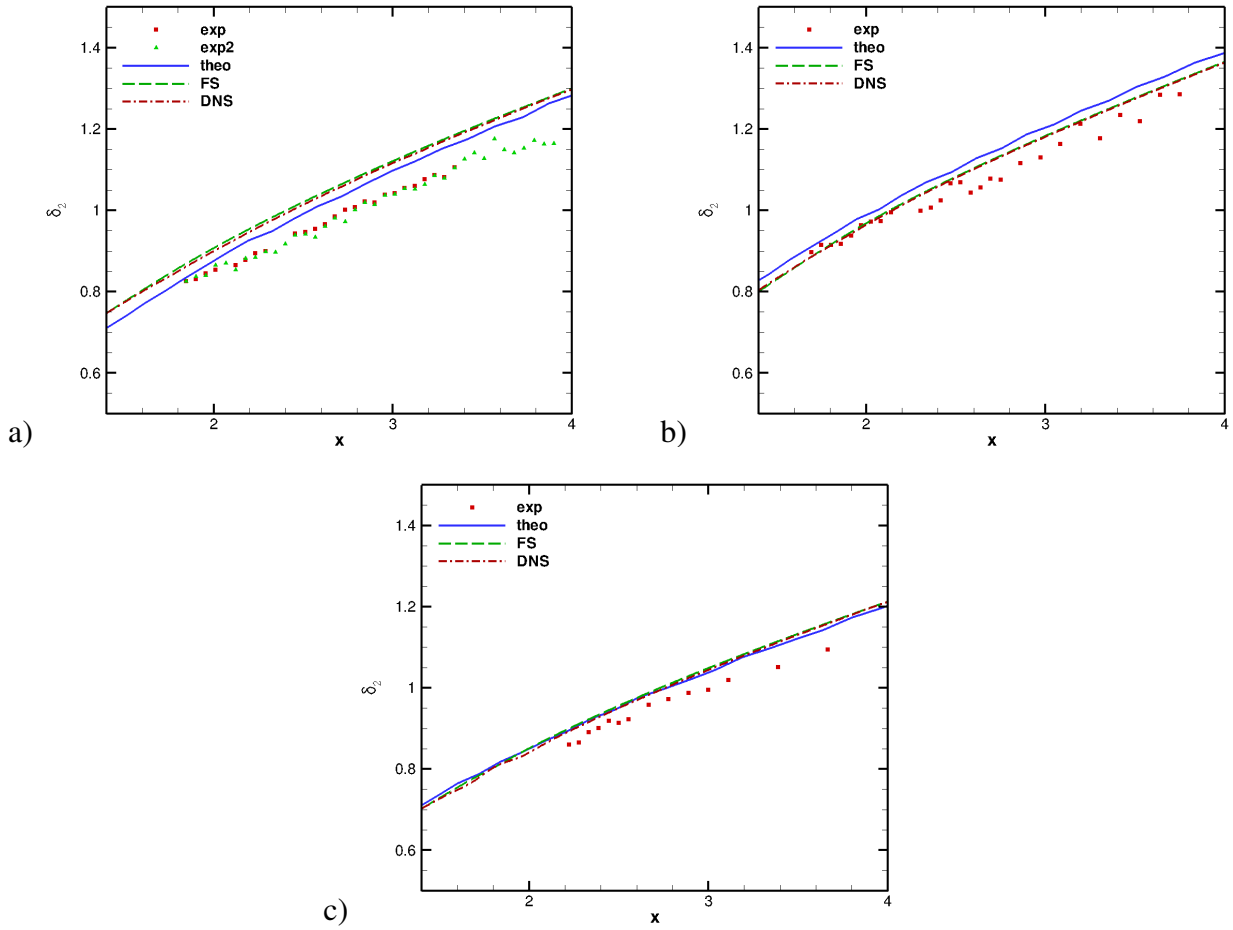

Figure 4. Momentum thickness δ_2 in streamwise direction x, a) flow with pressure gradient close to zero, b) decelerated flow, c) accelerated flow. Exp: experimental, theo: theoretical boundary layer profile, FS: Falkner-Skan solution, DNS: 2D-DNS result.

As for the displacement thickness, a similar behavior between experimental and numerical results can be noticed.

The last compared characteristic is the shape factor, which is the ratio between the displacement and momentum thicknesses:

$$H_{12} = \frac{\delta_1}{\delta_2}. \tag{38}$$

The streamwise variation of the shape factor for the cases considered is presented in Fig. 5. H_{12} and x values are non-dimensionalized by $\tilde{L}$.

One can see that the 2D-DNS results are closer to the experimental and calculated results than the FS ones. This is due to the simplifications done to obtain the Falkner-Skan equations. The 2D-DNS code removes the errors from this simplifications and can better represent the flow being simulated.

This results show that the 2D-DNS code was capable to simulate the flow according to the experimental results. This fact allowed the validation of this code.

4.2 Downstream development of modal amplitudes

After validating the code for the formation of the boundary layer, a linear stability test was made. For this test, a 2D-TS wave with small amplitude was introduced at the disturbance strip, located between x_1 and x_2 (see Fig. 1). This TS wave produces a disturbance in the velocity field and the amplitude of this disturbance in the streamwise component of the velocity was measured and compared. The amplitude of the TS waves is small enough to neglect the nonlinear products.

The comparison presented in this section involves the experimental results, the results obtained with a Linear Stability Theory (LST) code and the results of the three-dimensional DNS code.

The variation in the amplitude of the maximum value of the disturbance of the streamwise velocity component u over

ISSN 2176-5480

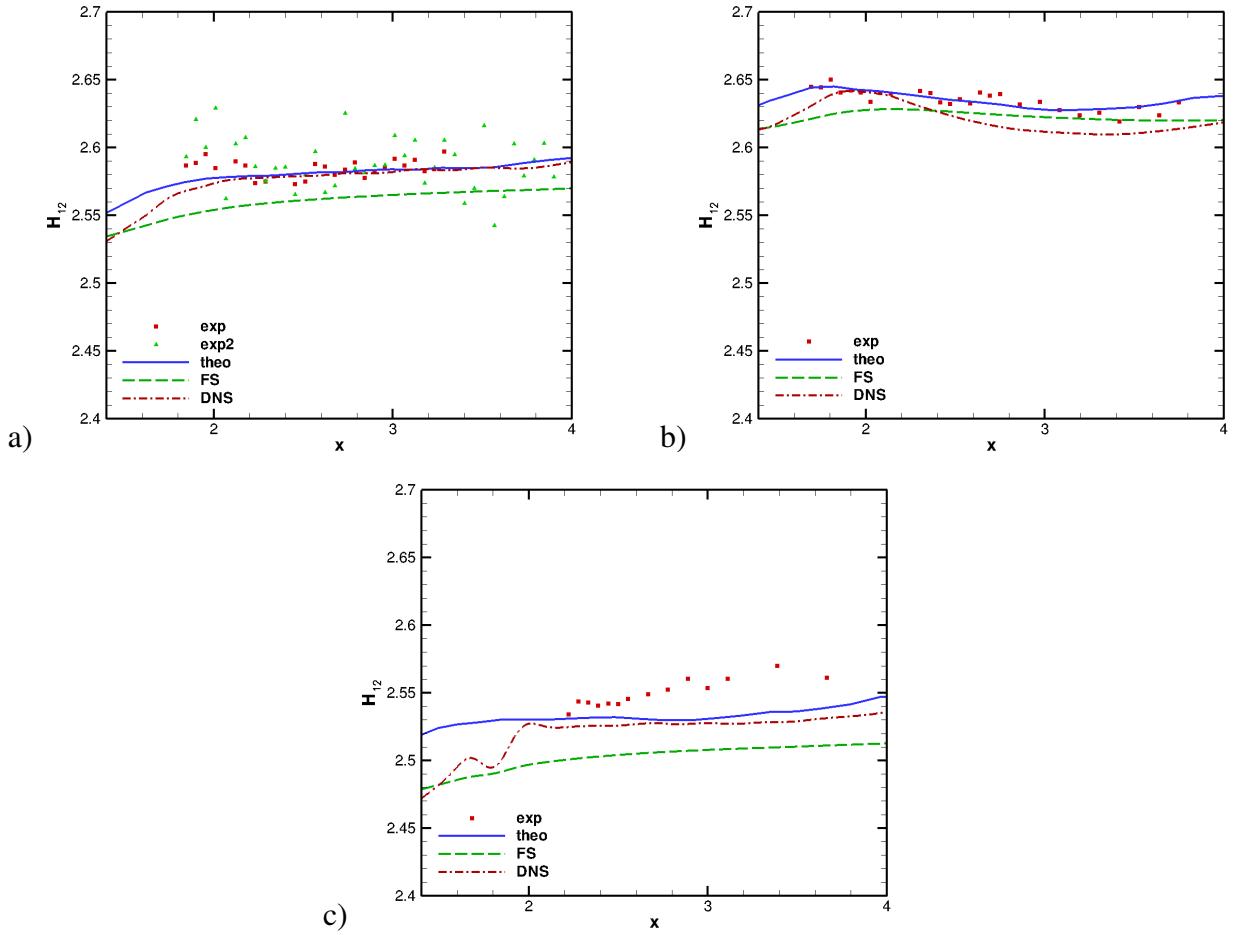

Figure 5. Shape factor H_{12} in streamwise direction x, a) flow with pressure gradient close to zero, b) decelerated flow, c) accelerated flow. Exp: experimental, theo: theoretical boundary layer profile, FS: Falkner-Skan solution, DNS: 2D-DNS result.

the wall-normal direction y, is defined as:

$$amp = \max_{y}(u'(1,0)), \tag{39}$$

where u' is the disturbance of the velocity.

The parameters used for the 3D-DNS code are the same as those for the 2D-DNS code, with wavelength in spanwise direction $\lambda_z = 0.4$m.

In these tests, two cases were considered: a flow with pressure gradient close to zero and a flow with adverse pressure gradient.

The first comparison was made taking into account the flow with pressure gradient close to zero. For this case a frequency of disturbance $F = 549$Hz is considered. Figure 6 shows the variation in the amplitude of the disturbance u' in streamwise direction x.

It can be noticed that the 3D-DNS numerical results agree with both the experimental and the LST code results.

For the flow with adverse pressure gradient, three frequencies were considered: $F = 396$Hz, 549Hz and 701Hz. Figure 7 shows the variation in the amplitude of the disturbance u' in streamwise direction for these cases.

Again, the DNS-3D results are very similar to the experimental and the LST code results.

5. CONCLUSION

The result presented above show that experimental data and numerical solution are in good agreement in the formation of the boundary layer. Experimental, LST and numerical results also agree in the disturbance of TS waves. Verification and validation of the DNS code are presented with this results.

This code is going to be used to predict the transition point of a boundary layer flow in a surface containing a roughness. Comparisons with experimental results will also be done.

ISSN 2176-5480

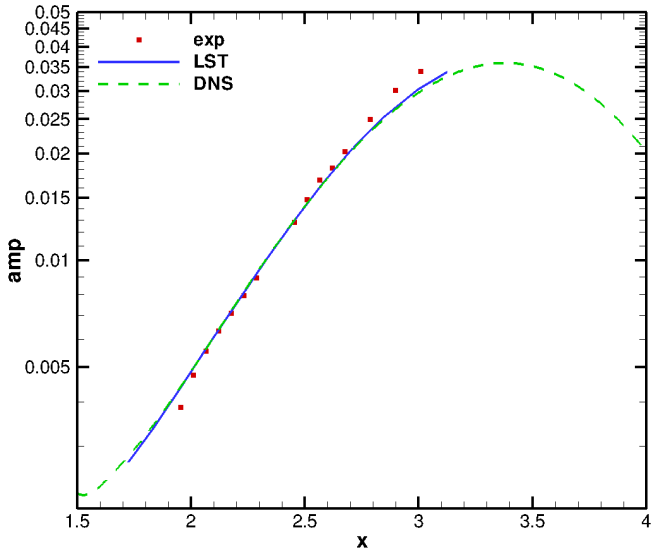

Figure 6. Amplitude of perturbation of the streamwise velocity component (amp - in log scale) in streamwise direction x for the flow with pressure gradient close to zero, with frequency $F = 549$Hz.

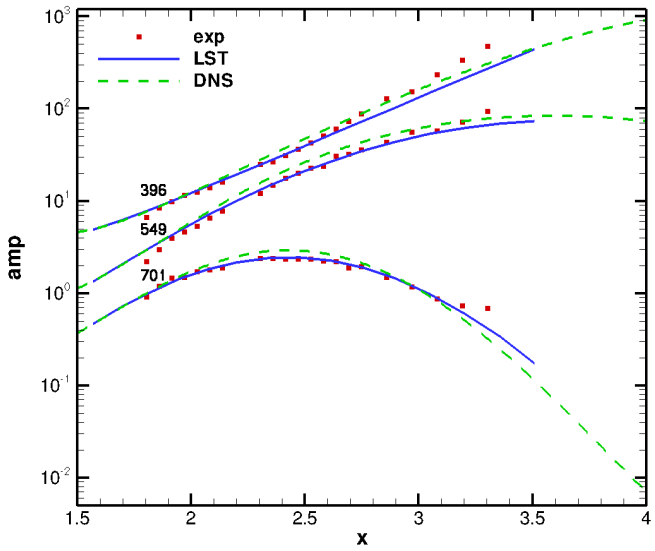

Figure 7. Amplitude of perturbation of the streamwise velocity component (amp - in log scale) in streamwise direction x for the flow with adverse pressure gradient, with frequencies $F = 396$Hz, 549Hz and 701Hz.

6. ACKNOWLEDGEMENTS

The authors acknowledge Benjamin Plogmann and Werner Würz for providing the experimental results and assistance in the analysis of the comparisons.

The authors also acknowledge the financial support received from FAPESP under grants 2010/00880-2 and 2011/19215-1.

7. REFERENCES

Cebeci, T. and Smith, A.M.O., 1974. *Analysis of turbulent boundary layers*. Academic Press, Inc.

Currie, I.G., 2003. *Fundamental Mechanics of Fluids*. Marcel Dekker, Inc.

Ferziger, J.H. and Peric, M., 1997. *Computational Methods for Fluid Dynamics*. Springer-Verlag Berlin Heidelberg New York.

ISSN 2176-5480

Kloker, M. and Konzelmann, U., 1993. "Outflow boundary conditions for spacial Navier-Stokes simulations of transition boundary layers". *AIAA Journal*, Vol. 31, pp. 620–628. doi:10.2514/3.11595.

Kloker, M.J., 1998. "A robust high-resolution split-type compact FD-scheme for spatial direct numerical simulation of boundary-layer transition". *Applied Scientific Research*, Vol. 59, No. 4, pp. 353–377. doi:10.1023/A:1001122829539.

Lele, S.K., 1992. "Compact finite difference schemes with spectral-like resolution". *Journal of Computational Physics*, Vol. 103, pp. 16–42. doi:10.1016/0021-9991(92)90324-R.

Meitz, H.L., 1996. *Numerical investigation of suction in a transitional flat-plate boundary layer*. Ph.D. thesis, University of Arizona.

Plogmann, B., Würz, W. and Krämer, E., 2012. "Interaction of a three-dimensional roughness element with a TS-wave near an airfoil leading edge". In *Procedings of the 16th International Conference on Methods of Aerophysical Research*. Kazan, Russia.

Reed, H.L., Saric, W.S. and Arnal, D., 1996. "Linear stability theory applied to boundary layers". *Annual Review of Fluid Mechanics*, Vol. 28, pp. 389–428. doi:10.1146/annurev.fl.28.010196.002133.

Souza, L.F., Mendonça, M.T. and Medeiros, M.A.F., 2005. "The advantages of using high-order finite differences schemes in laminar-turbulent transition studies". *International Journal for Numerical Methods in Fluids*, Vol. 48, pp. 565–582. doi:10.1002/fld.955.

Souza, L.F.d., 2003. *Instabilidade centrífuga e transição para turbulência em escoamentos laminares sobre superfícies côncavas*. Ph.D. thesis, Instituto Tecnológico de Aeronáutica.

Stüben, K. and Trottenberg, U., 1981. *Nonlinear multigrid methods, the full approximation scheme*, Köln-Porz, chapter 5, pp. 58–71. Lecture Notes in Mathematics.

White, F.M., 2006. *Viscous Fluid Flow*. McGraw-Hill.

8. RESPONSIBILITY NOTICE

The authors are the only responsible for the printed material included in this paper.